Sigma Journal of Engineering and Natural Sciences
Web page info: https://sigma.yildiz.edu.tr
DOI: 10.14744/sigma.2026.2047

Research Article

Dam-break analysis with infoworks ıcm model for earthquake-damaged Sultansuyu Dam: Different scenarios and computational costs

Burak ÇIRAĞ[1,*], Alp Ertuğrul ÖZER[2], Rıdvan KARAGÖZ[2], Bilal UTANCİK[3], Alaaddin Özgüray AYDIN[3], Mahmut FIRAT[4]

[1]*Department of Civil Engineering, Ataturk University, Erzurum, 25240, Türkiye*
[2]*Department of Civil Engineering, Istanbul, Istanbul Technical University, 34469, Türkiye*
[3]*Viasu Technology, Istanbul, 34774, Türkiye*
[4]*Department of Civil Engineering, Inonu University, Malatya, 44280, Türkiye*

ARTICLE INFO

Article history
Received: 04 July 2025
Revised: 14 October 2025
Accepted: 21 March 2026

Keywords:
Computational Costs; Dam-Break Analysis; Flood Hazard Maps; Flood Inundation Maps; Flood Velocity Maps; Infoworks ICM

ABSTRACT

Despite the many benefits of dams built for various purposes, their failure remains a serious risk due to the large volumes of water they store. The simulation of dam failure incidents is crucial for both emergency preparedness and risk mitigation strategies. This research conducts a dam-break analysis of the Sultansuyu Dam, which sustained significant damage during the earthquake that struck Türkiye on February 6, 2023, employing a hydrodynamic model formulated with the InfoWorks Integrated Catchment Modelling. Five distinct scenarios were crafted to assess both the computational cost and the dynamics of flooding behavior. There are four scenarios with complete reservoir condition (60 m) and velocity limits of 3, 5, 10, and 15 m/s, and the last one has a water depth of 50 m and a velocity limit of 15 m/s, indicating the depth at the time of the earthquake event. For each, flood inundation, velocity, and hazard maps were generated. Model validation with a historical rainfall event produced satisfactory performance (R^2 =0.772, NSE =0.467, RMSE =0.136 m). Results show that increasing the velocity limit causes the floodwater to move through narrower cross-sections, reducing overall inundation but increasing local flow depth. About 95% of flooded areas were classified as extreme hazard zones. Computational time increased by 1,219 seconds from the lowest to the highest velocity limit, indicating that lower limits require less computational effort. The study shows how velocity limits in hydrodynamic modeling affect flood hazard and computational efficiency, offering practical insights for dam safety and emergency planning.

Cite this article as: Çırağ B, Özer AE, Karagöz R, Utancık B, Aydın AÖ, Fırat M. Dam-break analysis with infoworks ıcm model for earthquake-damaged Sultansuyu Dam: Different scenarios and computational costs. Sigma J Eng Nat Sci 2026;44(2):1491–1508.

***Corresponding author.**
*E-mail address: burak.cirag@atauni.edu.tr

This paper was recommended for publication in revised form by Editor-in-Chief Ahmet Selim Dalkilic

INTRODUCTION

Dams are man-made structures that hold large amounts of water and are built for a variety of reasons, such as generating hydroelectricity, controlling floods, and providing irrigation water. But when these dams break, a lot of water flows downstream in the form of floods, which can cause terrible things to happen [1]. Earthquakes, wear and tear on the dam itself, overtopping, seepage, and other factors can cause these failures. When this happens, the dam can no longer hold the water pressure [2,3]. Moreover, Sesli and Akköse [4] assessed the sliding stability of concrete gravity dams in Turkey employing the Multiple Wedge Analysis method and determined that earthquake acceleration is a paramount factor influencing dam safety. Dam break flows generate rapid increases in water levels and a flood wave. These flows are highly unsteady and can exert significant forces on man-made structures such as bridges and buildings in their path, as well as entrain large amounts of bed material [5,6]. In order to reduce and prevent the impact of these damages, the risk status of the regions can be determined through flood inundation maps [7,8].

The rainfall-runoff relationship that may occur due to dam failure can be represented by 1D, 2D, or 3D hydrodynamic models depending on the structure of the surface water body to be modeled. Al-Salahat et al. [9] created flood inundation maps with dam-break scenarios using the Hydrologic Engineering Center-River Analysis System (HEC-RAS) for the Wadi Al-Arab Dam in Jordan. As a result of the study, the maximum estimated water depth for overtopping was 37.6 m and 26 m for piping failure. Abdulrahman et al. [10] has performed an effort to analyze the risk situation of downstream regions of the dam by using HEC-RAS 2D to model the break of the Khassa Chai Dam at Kirkuk. The result reflects that flood water will inundate the city center within one hour and will affect most metropolitan areas of the city. Musa et al. [11] aimed to identify the areas that would be affected by flooding in the event of the failure of the Sembrong Dam in Johor, Malaysia. Using InfoWorks ICM and geographic information systems (GIS) software, they created flood inundation maps and reported that the flood covered a distance of more than 20 km from the vicinity of Ayer Hitam town to Parit Raja. In addition, the flood depth obtained for this area varies between 0.5 and 1.2 m. Azeez et al. [1] used HEC-RAS-2D software to model the collapse of the Um Al-Khair dam in Jeddah, Saudi Arabia, which collapsed during a severe storm event in January 2011. They reported that the performance metrics measuring the agreement between observed and simulated water depths were Root Mean Square Error (RMSE) of 0.45 m and correlation coefficient of 0.57. Using hydrodynamic modeling often requires high computational costs to perform these simulations, which require thousands or millions of calculation points (or mesh elements) [12]. Graphics processing units (GPUs) have been used in recent years for high-resolution modeling to address the heavy computational loads [13]. In the same way, Tayfur et al. [14] used the RANS equations and the PISO algorithm to numerically simulate dam-break flows and sediment transport over movable beds. This showed how important it is to use efficient computational methods when modeling complicated flow-sediment interactions.

This study aims to perform a dam-break analysis for the Sultansuyu Dam in Malatya, Türkiye, which developed cracks in the dam body during the earthquake that severely affected Türkiye on February 6, 2023. This analysis is characterized by 5 different scenarios. There is no study in the literature (as far as the authors know) that incorporates the effect of computational costs in the analysis with different scenarios by setting a velocity limit. These scenarios were created by setting velocity limits of 3 m/s, 5 m/s, 10 m/s, and 15 m/s when the dam is full (60 m water height). In addition, the 5th scenario includes a velocity limit of 15 m/s according to the dam's water height of 50 m on the day of the earthquake. Flood inundation maps, flood velocity maps, and flood hazard maps were created for these 5 scenarios. For the 4 scenarios with velocity limits, the calculation times of the models run with the same conditions were compared. In addition, the model was validated with a historical rainfall event and evaluated with statistical performance evaluation criteria. Previous studies on dam-break analysis have mostly focused on hydraulic behavior and flood propagation, while relatively few have examined the influence of numerical parameters such as velocity constraints on computational performance. Furthermore, research that integrates earthquake-induced dam damage, scenario-based hydrodynamic modeling, and computational cost evaluation is still scarce. This study enhances the literature by consolidating these elements into a unified modeling framework and illustrating the application of velocity-limited hydrodynamic simulations to assess both model stability and performance efficiency. Although modern hydrodynamic solvers employ techniques such as adaptive time-stepping to satisfy the Courant-Friedrichs-Lewy (CFL) condition for numerical stability, high-velocity gradients in dam-break flows often lead to excessively small time steps, drastically increasing computational cost. In engineering practice, imposing artificial velocity limits is a common strategy to mitigate this issue. However, the trade-off between the computational gain from such limits and the resulting loss in physical accuracy (e.g., underestimation of flood extent) remains under-investigated. Therefore, this study also serves as a numerical experiment, quantifying how different velocity constraints influence both the solver's efficiency and the resultant hazard classification in a catastrophic failure scenario. The results are anticipated to facilitate subsequent research on risk-oriented dam safety evaluation and the enhancement of hydrodynamic models in scenarios with limited data availability.

MATERIALS AND METHODS

Study Area and Dam Characterıstıcs

Sultansuyu dam is an earth core sand gravel dam and was constructed between 1986 and 1992 on the Sultansuyu stream in the Tigris-Euphrates Basin in Malatya province in eastern Türkiye. Built for irrigation purposes, the dam contributes to agricultural production by providing water to 11,665 ha of land. According to the General Directorate of State Hydraulic Works (DSI), the height of the dam crest above sea level is 906 m, the body height from the foundation is 60 m and the length is 721 m. The reservoir capacity of the dam is 47.9 hm3 at normal operation level with a body volume of 3.205 hm3 and a lake area of 2.5 km2. In addition, the project flow rate is 1,050 m3/s [15]. The location of the dam is shown in Figure 1.

An earthquake of a magnitude of 7.8 (Mw) struck the Pazarcık district of Kahramanmaraş province in southeast Turkey on February 6, 2023, at 04:17 local time. Then, in the Elbistan region of Kahramanmaraş province, another earthquake with a magnitude of 7.6 (Mw) struck nine hours after the previous one. Over 50,000 people lost their lives and over 100,000 were injured as a result of these earthquakes, which hit Türkiye and Syria hard. The Republic of Türkiye declared a state of emergency in 11 provinces. In Malatya, one of the 11 provinces, more than 1,000 people were dead and nearly 10,000 injured. 345,536 houses were

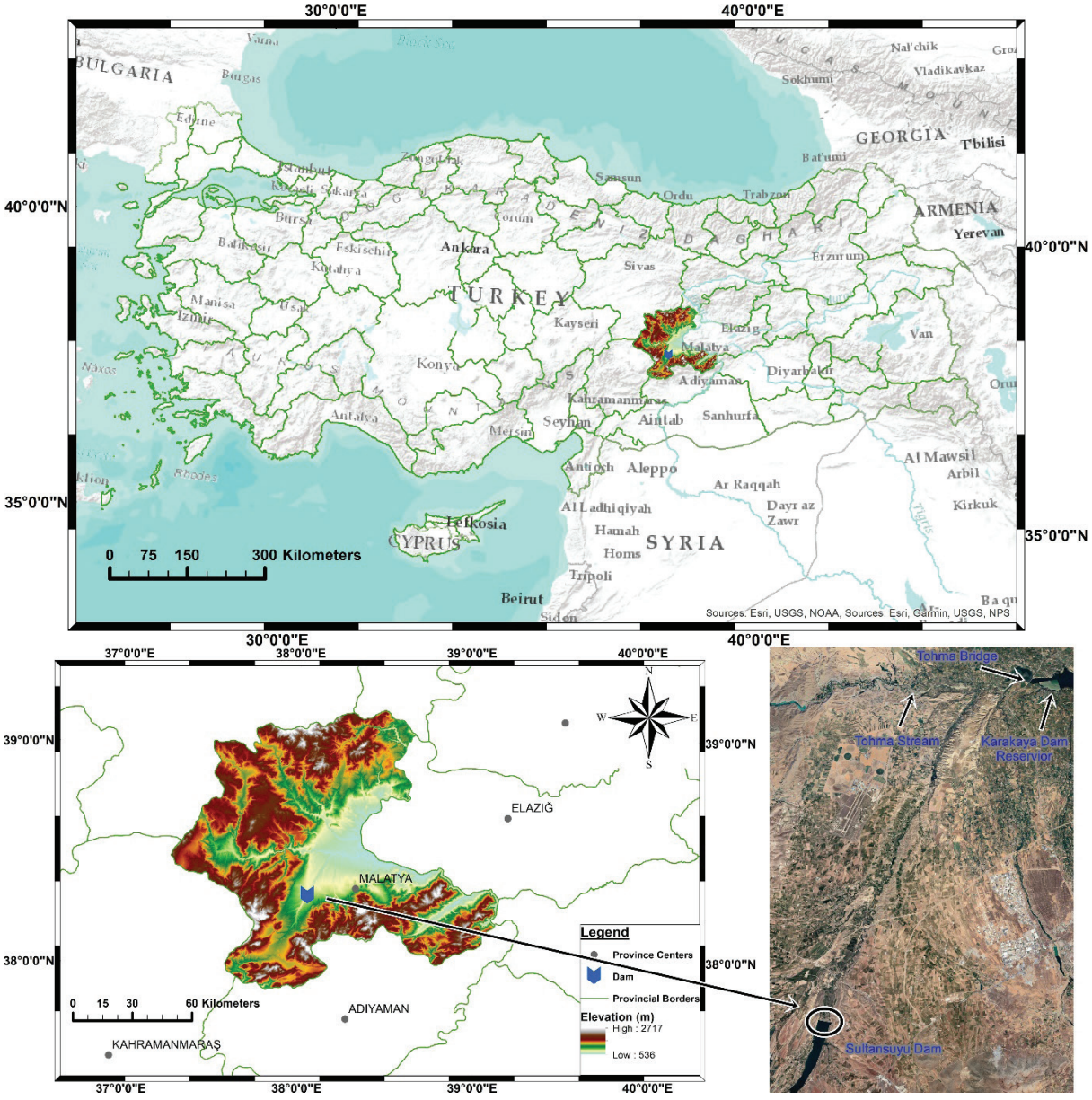

Figure 1. The location map of Sultansuyu Dam showing the reservoir area and downstream settlements.

damaged in Malatya and thousands of people were forced to migrate.

Due to these two earthquakes, 140 dams were subjected to moderate to high seismic intensity. Although all dams were able to maintain their water retention capability, moderate to large permanent deformations occurred in some of them. For this reason, water levels in Sultansuyu and Arıklıkaş dams were reduced in a controlled manner as part of emergency response measures [16].

Sultansuyu Dam, located in Akçadağ district of Malatya province, is 75 km from the epicenter of the Elbistan earthquake. During the earthquakes, the dam reservoir's water level was 50 meters, and the dam's crest and upstream slope developed large longitudinal cracks [17]. Transverse cracks were initially around 0.8-1.0 m, but after 10 days the depth of these cracks reached 4.0 m (Fig. 2) [18]. The Presidency of the Republic of Türkiye, Presidency of Strategy and Budget (SSB) published a report on the Kahramanmaraş earthquakes, stating that the Sultansuyu Dam was heavily damaged and the estimated damage cost was 705,000,000 Turkish Liras (Approximately 37 million dollars at the then exchange rate) [19]. In this context, Sultansuyu Dam was chosen as the study area because of the presence of settlements downstream of the dam and its critical importance for agricultural activities.

Methodology and Data Preparatıon

The methodology for assessing dam break analysis, as illustrated in Figure 3, begins with data collection and concludes with the analysis results. The first step is to obtain

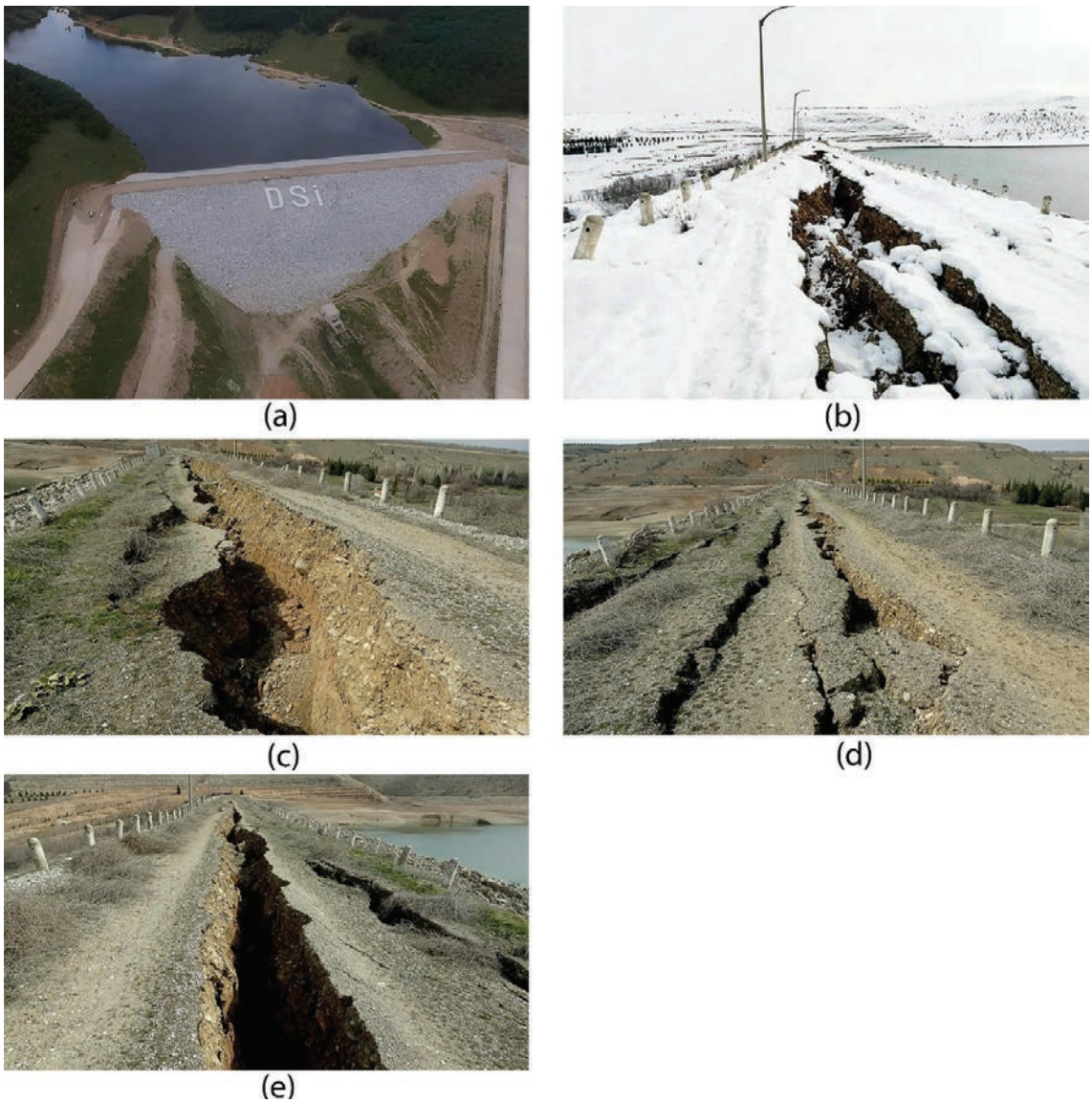

Figure 2. Views from Sultansuyu Dam: a) view of the dam before the earthquake (adopted from [20]); b)-e) view of damages on the dam body after the earthquake (adapted from [21,22]).

dam characteristics and isohypse maps from DSI. The isohypse maps were used to obtain digital elevation map (DEM) data from the topography of the empty dam reservoir. Meshing using the DEM data in InfoWorks ICM was performed using a minimum cell size of 25 m x 25 m near the dam and a minimum cell size of 100 m x 100 m in areas far from the dam. The spatial discretization of the domain was determined through a trade-off analysis between topographic precision and computational cost. The mesh size was varied from 25 m in the high-velocity zone immediately downstream of the dam to 100 m in the wider floodplain areas. This configuration was selected to match the resolution of the underlying digital elevation model (DEM), ensuring that the mesh captures the essential hydraulic features of the main channel without introducing artificial precision that exceeds the quality of the topographic data. Preliminary stability runs confirmed that this resolution is sufficient to resolve the flood wave propagation while maintaining computationally manageable runtimes. Coordination of Information on the Environment (CORINE) land cover data was obtained from the Republic of Türkiye Ministry of Agriculture and Forestry (TOB). These two data were arranged in ArcGIS environment for analysis in a way to be compatible with the study area and InfoWorks ICM program. The study area contains 7 different Manning's (n) values according to land use/cover classification (Table 1).

Then, the DEM data, dam reservoir, and 2D flow field were created in the hydrodynamic modeling program InfoWorks ICM. In this study, the dam break analysis was characterized according to different maximum flow velocities that would occur due to the dam break. These velocities are 3 m/s, 5 m/s, 10 m/s and 15 m/s. The maximum velocity in the 2D flow area is limited to these values. These velocity limits (3, 5, 10, and 15 m/s) are not randomly selected but are determined to represent the flow velocities observed in dam-break events in engineering. During an actual dam breach, the flow velocity can reach values in the range of 3-20 m/s within a short time, depending on factors such as breach geometry, water level difference, and downstream topography. However, the uncontrolled increase of these values within the hydrodynamic model leads to problems such as numerical instability and excessive computational cost. Therefore, different velocity limit scenarios were applied to achieve both behavior close to physical reality and numerical stability. Thus, the scenarios created reflect controlled conditions representing the velocity ranges that may be encountered in engineering. The model constrained by these velocities is represented with the assumption that the dam is full. In addition, the dam water level of 50 m on February 6, 2023, when the earthquake occurred, was added to the study as an extra scenario with a maximum velocity limit of 15 m/s. From the scenarios created according to these velocities, flood inundation maps, flood velocity maps, and flood hazard maps were provided. These maps can be viewed in InfoWorks ICM or any geographic information system (GIS) software.

Infoworks ICM Software And Dam Break Analyses

Floods caused by dam collapse can be predicted and depth and velocity estimates in the downstream valley can be obtained using mathematical hydrodynamic simulation models [9]. The present research used the InfoWorks ICM model with one-dimensional and two-dimensional modeling capabilities. For the dam-break analysis, 2D modeling based on meshing was used, which reflects the terrain topology and geometry and allows for more precise flow routing. InfoWorks ICM program includes the ability to solve the high computational cost of two-dimensional hydrodynamic modeling using GPU [23,24]. In the simulation setup, an instantaneous failure scenario was adopted as the breach mechanism. This approach assumes the immediate release of the entire reservoir water volume, representing a worst-case condition to analyze the downstream flood propagation dynamics.

The shallow water equation (SWE), a depth-averaged variant of the Navier-Stokes equations, serves as the foundation for the 2D engine in InfoWorks ICM. It is used to depict 2D flow mathematically [25,26]. The SWE presumes that the movement is primarily horizontal and that changes

Table 1. CORINE land use/cover distribution of the study area

Label	Manning's (n)	Area (km²)	Percent (%)
Airports, industrial or commercial units, etc.	0.013	9.524	2.28
Sparsely vegetated areas	0.027	9.816	2.35
Non-irrigated arable land, permanently irrigated land	0.030	109.563	26.19
Pastures	0.035	2.584	0.62
Complex cultivation patterns, etc.	0.040	173.556	41.49
Land principally occupied by agriculture, with significant areas of natural vegetation, etc.	0.050	22.751	5.44
Fruit trees and berry plantations, vineyards	0.080	90.492	21.63
Total		**418.286**	**100**

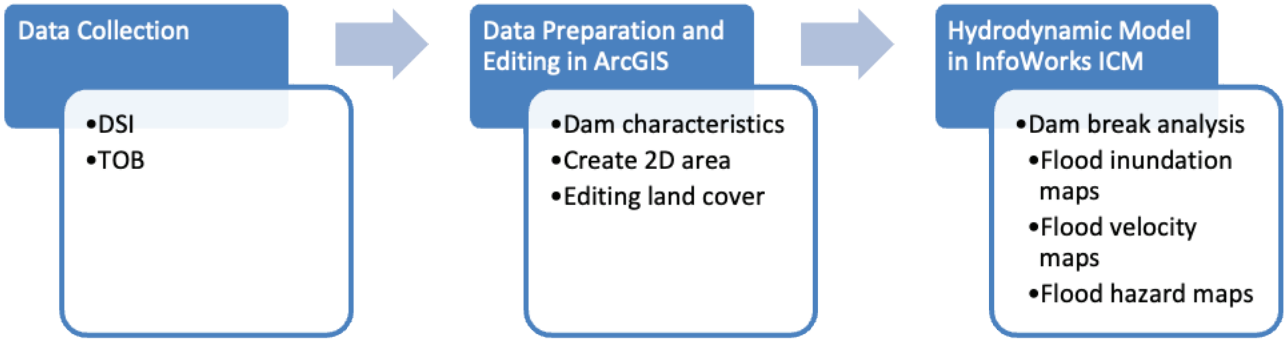

Figure 3. Methodology of the study.

in velocity along the vertical axis can be disregarded. InfoWorks ICM employs a conservative approach to solve the SWE, as described below [27]:

$$\frac{\partial h}{\partial t}+\frac{\partial (hu)}{\partial x}+\frac{\partial (hv)}{\partial y}=\sum_{i=1}^{n} q_i \tag{1}$$

$$\frac{\partial (hu)}{\partial t}+\frac{\partial}{\partial x}\left(hu^2+\frac{gh^2}{2}\right)+\frac{\partial (huv)}{\partial y}-\frac{\partial}{\partial x}\left(\varepsilon h\frac{\partial u}{\partial x}\right)-\frac{\partial}{\partial y}\left(\varepsilon h\frac{\partial u}{\partial y}\right)=gh\left(S_{0,x}-S_{f,x}\right)+\sum_{i=1}^{n} q_i u_i \tag{2}$$

$$\frac{\partial (hv)}{\partial t}+\frac{\partial}{\partial y}\left(hv^2+\frac{gh^2}{2}\right)+\frac{\partial (huv)}{\partial x}-\frac{\partial}{\partial x}\left(\varepsilon h\frac{\partial v}{\partial x}\right)-\frac{\partial}{\partial y}\left(\varepsilon h\frac{\partial v}{\partial y}\right)=gh\left(S_{0,y}-S_{f,y}\right)+\sum_{i=1}^{n} q_i v_i \tag{3}$$

The following terms represent various variables related to fluid dynamics or hydrodynamic modeling: h is the water depth (m); u and v are the velocities in the x and y directions (m/s), respectively; q_i is the net discharge per unit area from the ith source (m/s); u_i and v_i are the velocity components in the x and y directions of the ith discharge (m/s); g is the gravitational acceleration (m/s²); ε denotes eddy viscosity (m²/s); $S_{0,x}$ and $S_{0,y}$ represent the bed slopes in the x and y directions (m/m); $S_{f,x}$ and $S_{f,y}$ refer to the friction slopes in the x and y directions (m/m); and n indicates the total number of discharge sources. These variables are typically used to describe the movement of water, accounting for various forces such as gravity, friction, and external discharges, in models of fluid flow.

To ensure numerical stability and reproducibility, the simulation parameters were configured as follows: The simulation was run with a maximum computational time step of 5 seconds, subject to a timestep stability control factor of 0.95 to dynamically adjust for high-velocity flows. The semi-implicit weighting factor (Theta) was set to 0.9 to dampen numerical oscillations, and the inundation mapping depth threshold (wetting/drying limit) was defined as 0.01 m. For the downstream boundary condition, a fixed water level representing the reservoir level of the Karakaya Dam was applied to simulate the hydraulic backwater effect at the confluence point. Spatially distributed Manning's roughness coefficients were applied based on the CORINE land cover classification (as detailed in Table 1).

The maximum flood hazard rating, which depends on depth and velocity, is used by InfoWorks ICM to compute the hazard values. This value is calculated with the equation proposed by the Defra/Environment Agency of the United Kingdom [28,29].

$$HR=d(v+1.5)+DF \tag{4}$$

where HR is the (flood) hazard rating, d is the depth of flooding (m), v is the velocity of floodwaters (m/sec) and DF is the debris factor. The classification of the ratios according to the degree of hazard is given in Table 2.

Table 2. Classification of hazard values (adapted from [28])

Rate	Degree of Flood Hazard	Description
<0.75	Low	Caution
0.75-1.25	Moderate	Dangerous for some (i.e. children)
1.25-2.5	Significant	Dangerous for most people
>2.5	Extreme	Dangerous for all

In the calculation of the Hazard Rating, the Debris Factor (DF) was assigned dynamically based on the standard DEFRA methodology implemented in InfoWorks ICM. Accordingly, a value of 0.5 was applied for flood depths less than 0.25 m, and a conservative value of 1.0 was applied for depths exceeding 0.25 m.

Model Performance Evaluatİon

A suggested model's intricate parts and few observations make it challenging to validate and calibrate. 2D analyses such as flood and landslide simulations can be validated using available observational data [30]. In this study, three statistical indicators, the coefficient of determination (R^2), Nash-Sutcliffe efficiency (NSE) [31], and Root-mean-square error (RMSE), were used to determine the agreement between observed flood depth and modeled flood depth values. R^2 ranges from 0 to 1 and indicates how well the model explains the variance of the dependent variable, with higher values representing better model fit and satisfactory performance when exceeding 0.5 [32-34]. NSE is a measure used to validate models involving hydrological phenomena [35]. NSE values between 1.0 and 0.8 are considered excellent, between 0.8 and 0.6 are regarded as good, and between 0.6 and 0.05 as satisfactory. Additionally, NSE values ranging from 1.0 to 0 are deemed acceptable [26]. RMSE can be any number between 0 and ∞, and lower values mean the model is doing better. It tells you how big the errors are on average between the observed and simulated values. An RMSE of 0 means that the model is perfect and has no errors [36]. The equations for the statistical evaluation criteria are given below.

$$R^2 = \frac{\sum_{i=1}^{n}(x_i - x_{avg})^2 - \sum_{i=1}^{n}(x_i - y_i)^2}{\sum_{i=1}^{n}(x_i - x_{avg})^2} \quad (5)$$

$$NSE = 1 - \left[\frac{\sum_{i=1}^{n}(x_i - y_i)^2}{\sum_{i=1}^{n}(x_i - x_{avg})^2}\right] \quad (6)$$

$$RMSE = \sqrt{\frac{\sum_{i=1}^{n}(x_i - y_i)^2}{n}} \quad (7)$$

where xi represents the observed values, yi denotes the output values produced by the model, xi-yi indicates the error values, xavg is the average of the observed values, n is the number of data points.

RESULTS AND DISCUSSION

Statistical Evaluation of Model Results

About a month and a half after the earthquake that seriously affected the study area and Sultansuyu Dam, a heavy rainfall event occurred in the region where Sultansuyu Dam is located. The rainfall started on 13/03/2023 at 12:00, stopped in places, and continued until 16/03/2023 at 05:00, flooding areas such as living areas and orchards near the dam. The excessive rains caused certain roadways above and downstream of the dam to be restricted to both human and vehicular traffic. On one of these highways, some measured values were obtained as a result of reports by local people and news channels. When these measured values were compared with the values measured in the model, the statistical evaluation criteria R^2=0.772, NSE=0.467, and RMSE= 0.136 m were obtained. These results show that the model used is satisfactory. In hydrological modeling of ungauged or data-scarce regions, a positive NSE value indicates that the model provides better predictive skill than the mean observed value [37]. Considering the high uncertainty in observation data derived from limited field reports, these results are deemed satisfactory for emergency flood propagation analysis. Azeez et al. [1] utilized analogous validation methodologies in their simulation of the Um Al-Khair dam breach in Jeddah, Saudi Arabia, where the correlation coefficient (R^2 = 0.57) and RMSE (0.45 m) between observed and modeled water depths were deemed satisfactory under constrained field data circumstances, thereby affirming the credibility of such hydrodynamic modeling techniques in data-deficient areas. However, it is important to explicitly acknowledge that the validation process was constrained to a single rainfall-runoff event due to the scarcity of available hydrometric data in the

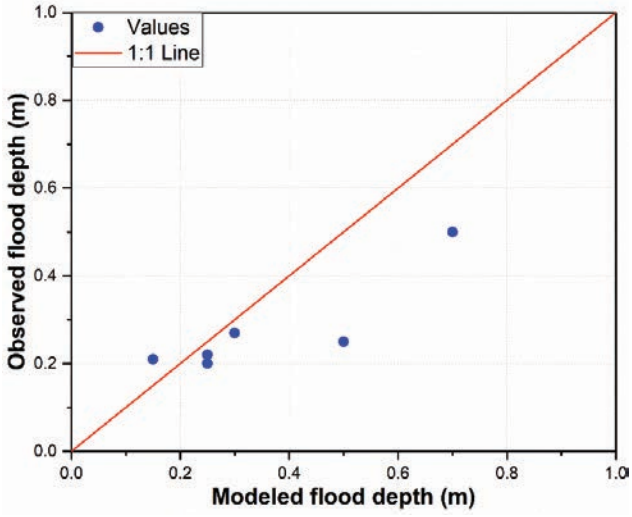

Figure 4. Scatter plot for comparison between the observed and modeled flood depths at some locations.

post-disaster period. The Sultansuyu Dam is in a rural area and doesn't have a lot of hydrometric observation stations, thus the model calibration process couldn't be done. Even though this situation is a problem because of a lack of data, the fact that the validation phase employed only one rainfall event shows that the model can give credible findings in similar hydrological situations. The model validation procedure, which uses a scenario-based analysis comparing technique, lessens the effect of calibration problems on the results' reliability. So, using the same model parameters in all circumstances keeps the results easy to understand. A scatter plot was made to show how the observed values and the modeled values for the historical rainfall event were related. This was done to see how well the model worked (Fig. 4).

Figure 4 shows the observed and modeled flood depths and a 45-degree line of agreement showing the line of perfect fit. All but one of the points are located below the line, indicating that the measured flood depths in the model are lower than the observed flood depths. According to the results of the statistical evaluation criteria and scatter plots, the model was found to have a good correlation in prediction.

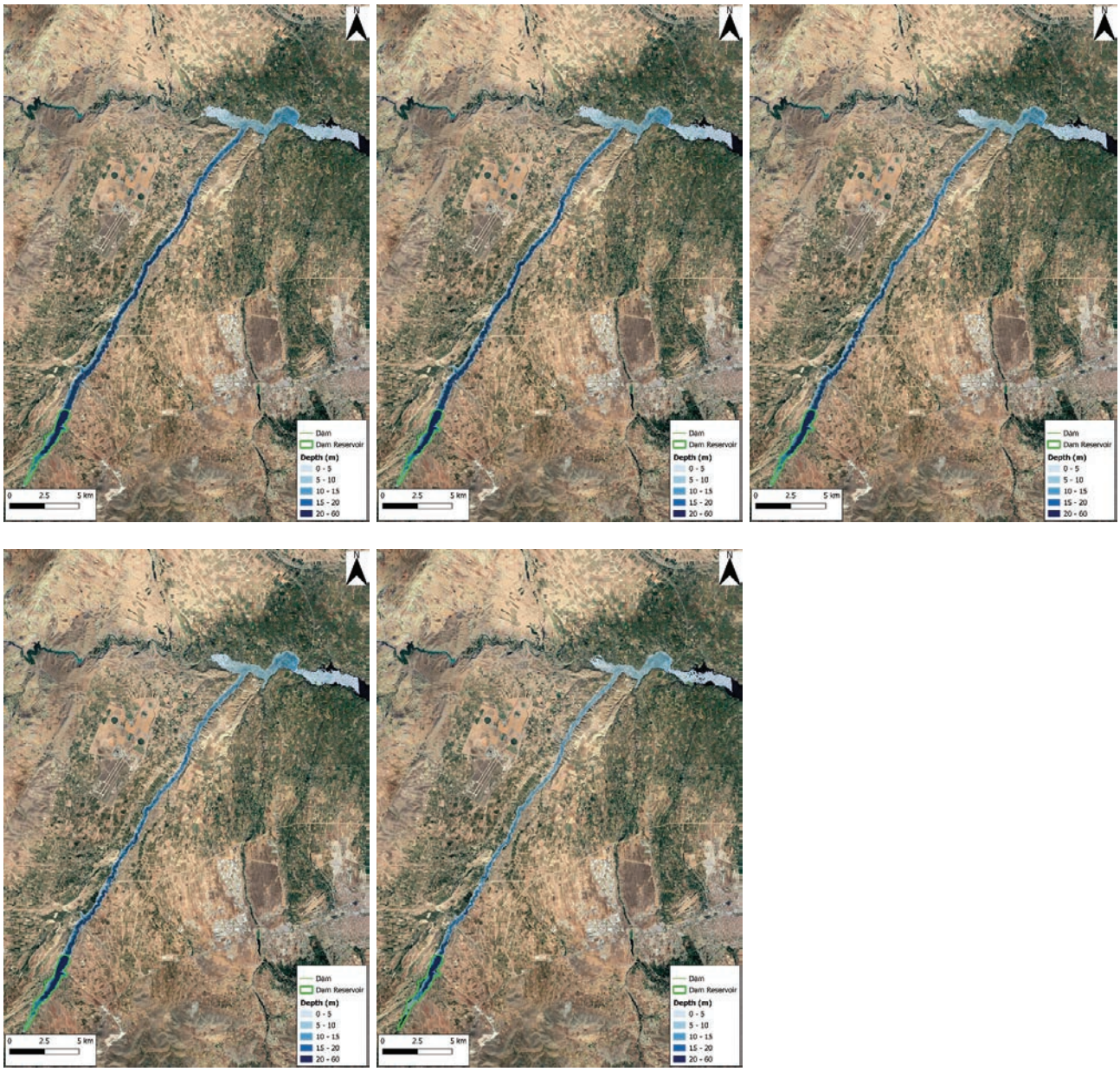

Figure 5. Flood inundation maps created according to maximum velocity limits and dam water height as a result of dam collapse: **a)** 3 m/s, **b)** 5 m/s, **c)** 10 m/s and **d)** 15 m/s maximum velocity limit for 60 m dam levels, **e)** 15 m/s maximum velocity limit for 50 m dam levels.

Finally, apart from the validation constraints, this study entails inherent uncertainties associated with the input parameters and modeling assumptions. First, the observation data used for validation were derived from field reports and visual evidence rather than gauge measurements, introducing a degree of uncertainty in the exact water depths. Second, the dam breach mechanism was simulated as an instantaneous failure to represent the worst-case scenario; however, a gradual erosion process might yield different peak timing and attenuation characteristics. Third, the roughness coefficients were assigned based on standard CORINE land cover classes without spatially distributed calibration. Despite these uncertainties, the conservative approach adopted herein ensures that the resulting hazard maps provide a safety margin suitable for emergency planning.

Flood Inundation Maps

In dam break analyses, the potential extent of damage resulting from a dam failure is closely linked to the topographical features of the surrounding land. For this reason, in order to accurately estimate the damage that may occur, the models are made with DEM maps that represent the topography of the land. With InfoWorks ICM, flood inundation maps can be created as a result of meshing using DEM maps [38]. In flood inundation maps, the probable magnitude and depth of floods due to dam break analysis are evaluated, giving meaningful information regarding the extent and the flood severity. Similarly, the maps assist to determine and examine probable flood consequences through the identification of the areas that are subjected to inundation. In the implementation of the strategies to assist minimize flood risk and increase the resilience of the populace to the occurrence of the natural hazard, the emergency managers, policymakers, and the urban planners can all gain through the delineation of the areas of inundation [9]. In this context, flood inundation mapping forms the first and most critical step of spatial impact assessment in dam-break studies. It enables the identification of inundation boundaries, spatial variation in flood depth, and the relationship between topography and flow concentration. Figure 5 shows the flood inundation maps generated as a result of the dam break analysis for maximum allowable velocities of 3 m/s, 5 m/s, 10 m/s, and 15 m/s assuming that the dam is full and 15 m/s when the water level of the dam is 50 m.

The upper bound is situated at the reservoir's dam position, and the flow process of the dam break simulation is used as the input condition for the flood simulation [39]. In the present study, villages downstream of the dam were found to be inundated under all the conditions considered.

For the scenario with a velocity limit of 3 m/s, 21.09 km2, for 5 m/s, 20.51 km^2, for 10 m/s, 19.29 km^2, for 15 m/s, 18.87 km^2 and for the velocity limit of 15 m/s at 50 m water height, 15.18 km^2 were flooded. In this context, in a 2D analysis, it can be said that the inundated area decreases as the velocity limit set for each grid cell increases. Similar patterns were observed by Khosravi et al. [40] in the Sefid-Roud Dam case study in Iran, where 2D HEC-RAS simulations showed that flood depth and extent decreased rapidly with distance from the dam and that the valley topography strongly controlled the concentration of floodwaters along the main flow path. In addition, the lowering of the dam water height has also reduced the inundation area. In

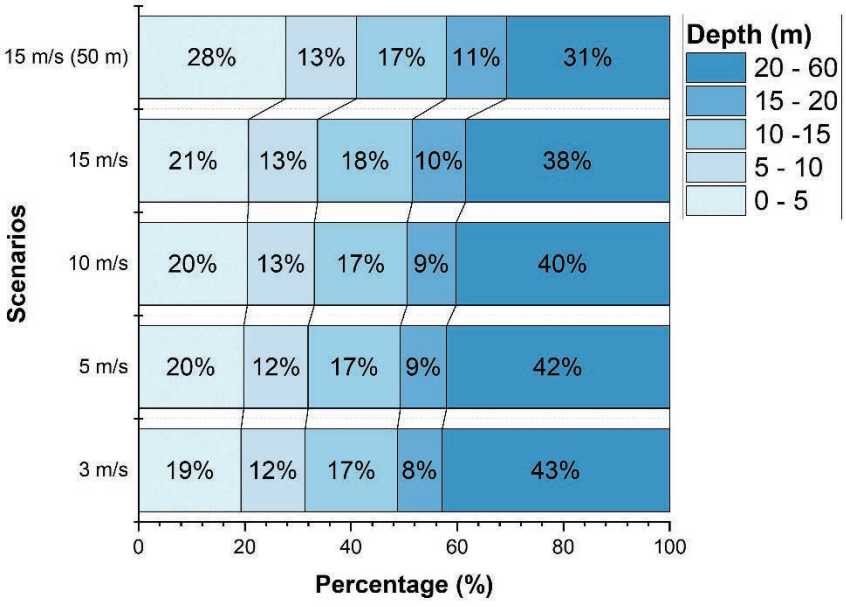

Figure 6. Proportional (%) distribution of areas covered by maximum water depths observed in the flood zone downstream of Sultansuyu Dam.

addition, due to the flood water from the dam break of the Sultansuyu Dam reaching the area where the Tohma stream and Karakaya Dam reservoir are located, settlements and agricultural lands located at the junction point are flooded. Accordingly, a possible dam-break event poses a great danger to urban man-made areas and the natural environment. Loss of life is likely to occur in the region, which includes mostly agricultural areas, for each scenario. Percentage values of inundation area according to the depths of the scenarios are given in Figure 6.

As the maximum velocity limit decreased in the scenarios, the percentage of high-water depths in the inundation areas increased (Fig. 6). In other words, the increase in maximum velocity limits led to a decrease in depths. In light of these results, the study emphasizes the importance of giving the correct velocity limit and adjusting the input conditions more accurately in modeling applications.

When it comes to apricot production, Turkey leads the world. Malatya accounts for over 85% of Turkey's dried apricot output and 55% of its fresh apricot production. Exports account for a significant portion of the dried apricot

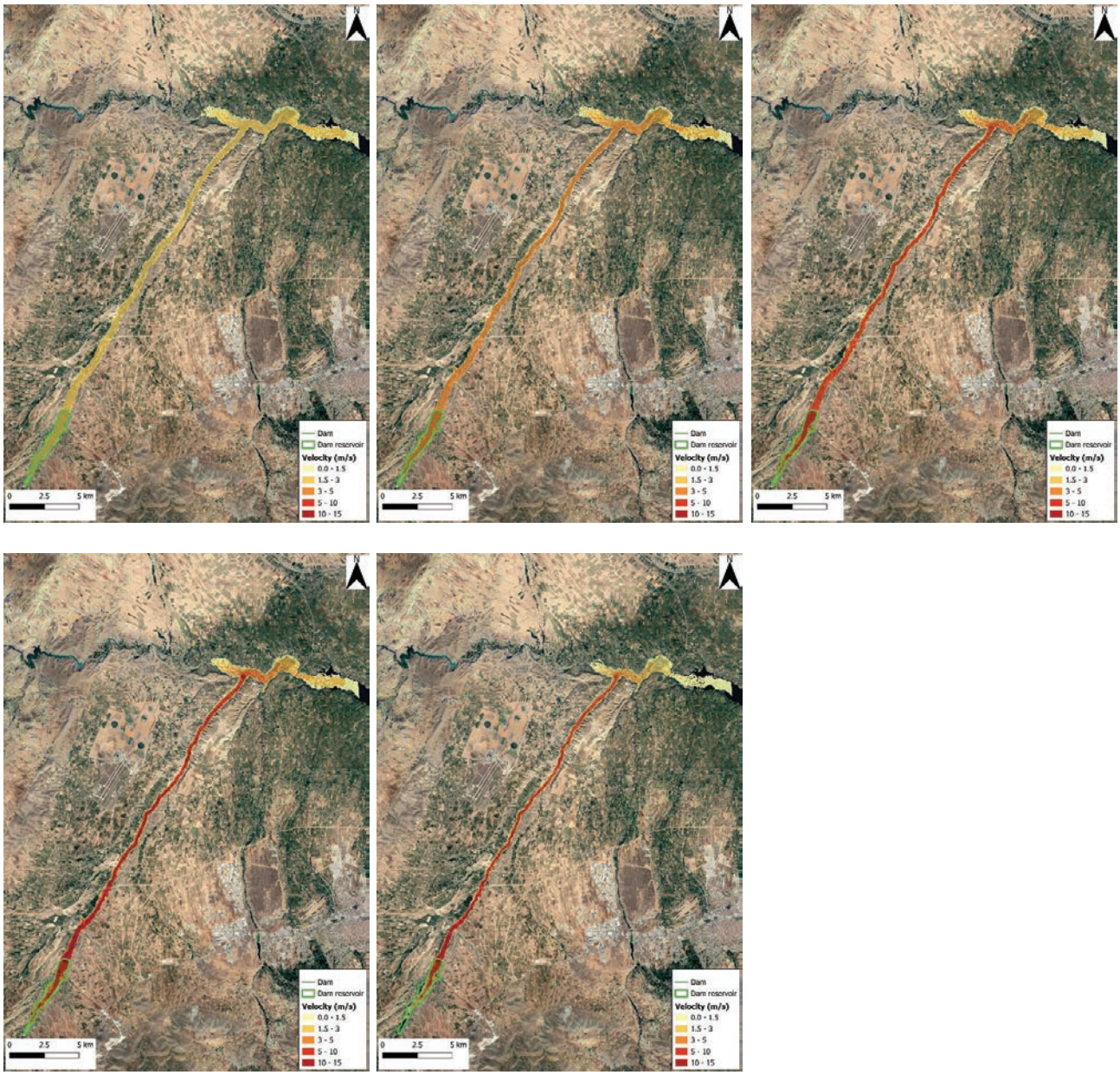

Figure 7. Flood velocity maps created according to maximum velocity limits and dam water height as a result of dam collapse: a) 3 m/s, b) 5 m/s, c) 10 m/s and d) 15 m/s maximum velocity limit for 60 m dam levels, e) 15 m/s maximum velocity limit for 50 m dam levels.

production [41]. Therefore, according to the outputs of the study, it can be said that the flooding of agricultural areas will negatively affect Türkiye socially and economically.

In addition, in all 5 scenarios, the water discharged from the dam quickly discharges to the place where the Tohma stream empties into the Karakaya Dam reservoir. As a result of the analysis, the flood water rapidly discharged into the dam lake increases the water level and floods the transportation roads (Tohma bridge) and the businesses located on the water's edge.

Flood Velocity Maps

In this study, 5 different scenarios based on the previously mentioned velocity limits and dam levels were created for the meshed 2D zone in InfoWorks ICM. An additional output from these scenarios is the flood velocity maps, whereby the flow movement of the flood wave is presented for the whole basin as the outcome of the analysis for dam break. The peak flood velocity is affected by a variety of aspects, such as the basin topographical attributes, the meandering course of the river, and the Manning's n coefficients [42]. Here, the flood velocity maps are important for the analysis of the dynamic attributes of the flood wave, the identification of the areas under high-velocity flow, and the evaluation of areas at risk for the infrastructures and the populations. The generated flood velocity maps are presented at Figure 7.

For all five scenarios, when the flood wave empties into the Karakaya Dam, it creates a flood effect. Accordingly, it poses a great danger to urban man-made areas and the natural environment. For the 3 m/s, 5 m/s, and 10 m/s velocity-limited scenarios, the velocity values mostly reach the maximum velocity level downstream of the dam. In this context, the dam break analysis for this dam and geographical features shows that more than these velocities will occur. For this reason, the analysis was also performed according to the 15 m/s velocity limit and it was seen that the velocities did not exceed 15 m/s (Fig. 7). Therefore, it is more likely that the velocity profile for a possible Sultansuyu Dam break will be as in 15 m/s. At 50 m dam water level height, the analysis showed that the velocities did not exceed the 15 m/s limit and progressed faster in a narrower area compared to the 10 m/s scenario. In other words, as the velocity limit increases in the scenarios based on the failure of the Sultansuyu dam, the inundation area decreases but the velocity increases. This is because the topography of the land has a channel structure sloping towards the Karakaya Dam reservoir. The higher the velocity, the greater the problem for people and the environment. Because a rapidly advancing flood wave will reduce the effects of disaster preparedness and make it more difficult to move away from risky areas. The areal percentages of the velocities for all scenarios are given in Figure 8.

As the maximum velocity limit value increases, the velocity values in the inundation intervals are clustered in the velocity limit region (Fig. 8). For this reason, velocities are generally at the upper limit at velocity limits of 3 m/s, 5 m/s, and 10 m/s. However, a more consistent distribution is observed at 15 m/s. Therefore, it is more likely that a result similar to that at the 15 m/s velocity limit will occur in the possible permanent break of the Sultansuyu Dam. Another proof of this is that the spatial percentage distribution of 0-1.5, 1.5-3, and 3-5 m/s velocities in the 10 m/s and 15 m/s scenarios are identical. In addition, when the water

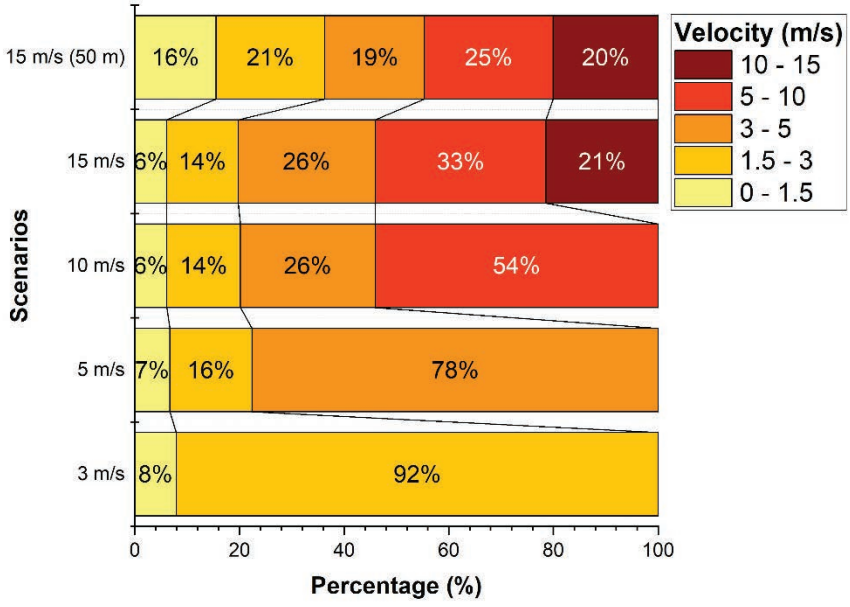

Figure 8. Proportional (%) distribution of inundated areas classified by maximum water velocity categories in the downstream flood zone.

height at the dam is reduced from 60 m to 50 m, there is an increase in low velocities. However, there is a small change in the high-velocity limits due to the high velocities at the point where the land is connected to the Karakaya Dam. The imposition of a maximum velocity limit acts as an artificial energy dissipation mechanism, effectively restricting the kinetic energy available to the flood wave at the advancing front. Consequently, this reduction in momentum flux prevents the flow from overcoming topographic resistance in distal areas, thereby resulting in narrower inundation extents compared to unconstrained simulations.

Flood Hazard Maps

Characterizing the depth and velocity at the water downstream of the dam also facilitated the generation of flood hazard maps. The classification highlighted in Table 1 served the basis for the flood hazard map generated for the subject study. The flood hazard mapping integrates both the depth and velocity data to determine the probable risk to people, infrastructures, and agricultural land, facilitating delineation of areas with very high risk within the floodplain. The flood hazard maps for 5 different scenarios are presented in Figure 9.

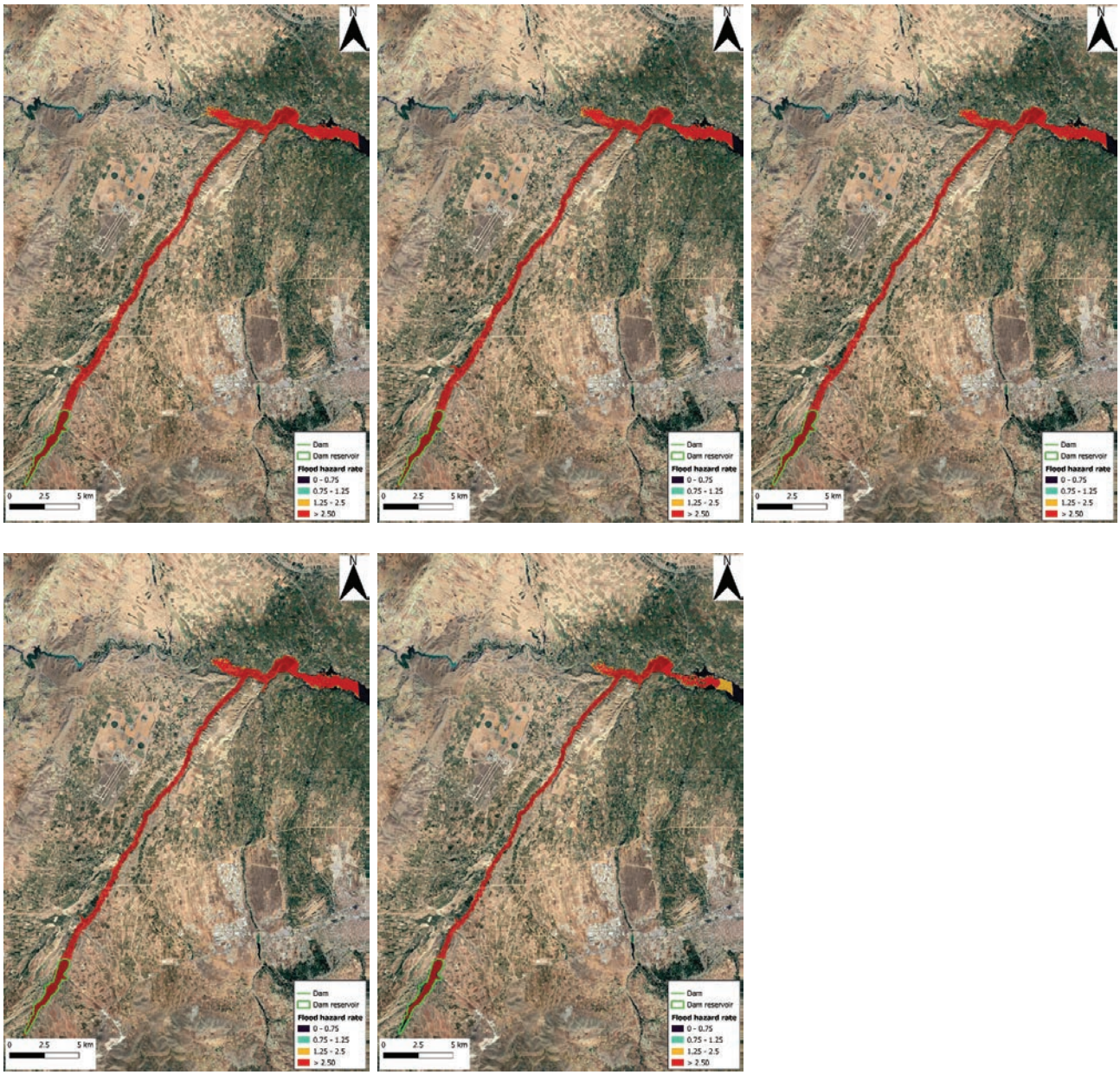

Figure 9. Flood hazard maps created according to maximum velocity limits and dam water height as a result of dam collapse: a) 3 m/s, b) 5 m/s, c) 10 m/s and d) 15 m/s maximum velocity limit for 60 m dam levels, e) 15 m/s maximum velocity limit for 50 m dam levels.

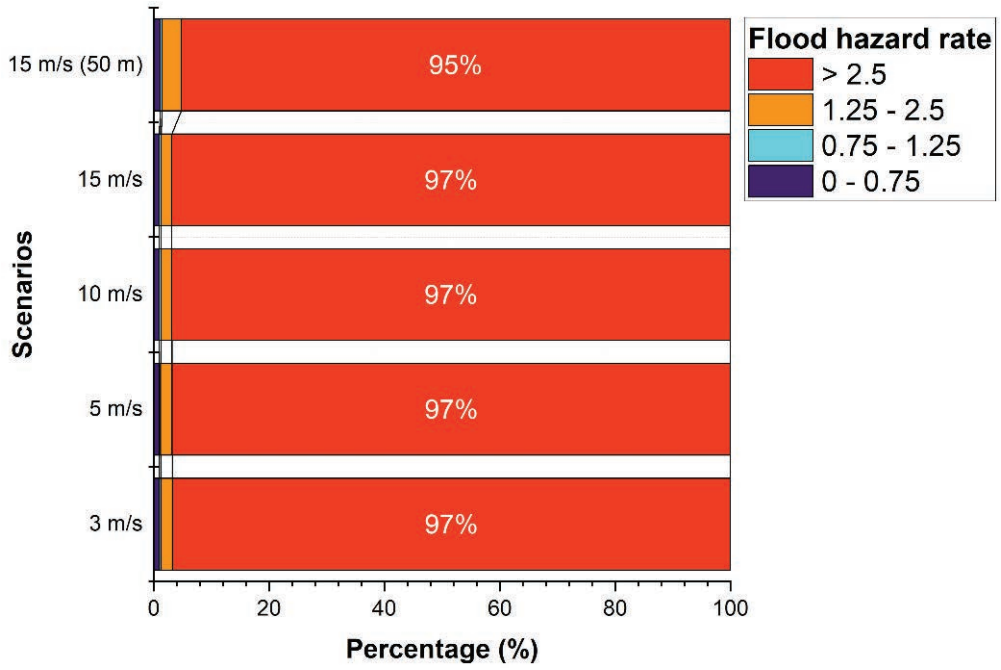

Figure 10. Proportional (%) distribution of the flood inundation area classified by calculated hazard level.

As a result of the study, for all five scenarios, each flood-affected area has an extreme flood level. According to this flood level, everyone is in danger in such a situation. This is because the depth and velocity of the flood water are quite high in this region. This is because the height of the downstream of the dam above sea level is gradually decreasing and the flood moves along a channel. Thus, the flood water moves in a strip without spreading around and reaches the extreme hazard level for each region. Percentage values and changes of flood hazard ratios according to inundation area are given in Figure 10.

Dam failures present significant risks due to the combination of high flow depths and velocities. In the case of the Sultansuyu Dam breach analysis, the resulting flow, characterized by both high velocity and depth, posed considerable threats to life and property within the affected flood zones. Consequently, the flood hazard index, which is determined by both depth and velocity, reached its peak value across nearly all inundated areas (Fig 10). Since the majority of the dam-break flood wave exhibits depths significantly larger than 0.25 m, the analysis effectively accounts for the high debris potential (DF=1.0) characteristic of such catastrophic events, thereby reinforcing the extensive 'Extreme Hazard' classification observed in the domain.

Results in Settlements

There are rural living areas in the downstream areas of Sultansuyu Dam. Livestock breeding and agricultural production are quite common in these areas. Within the scope of this study, the regions where the human factor is intense

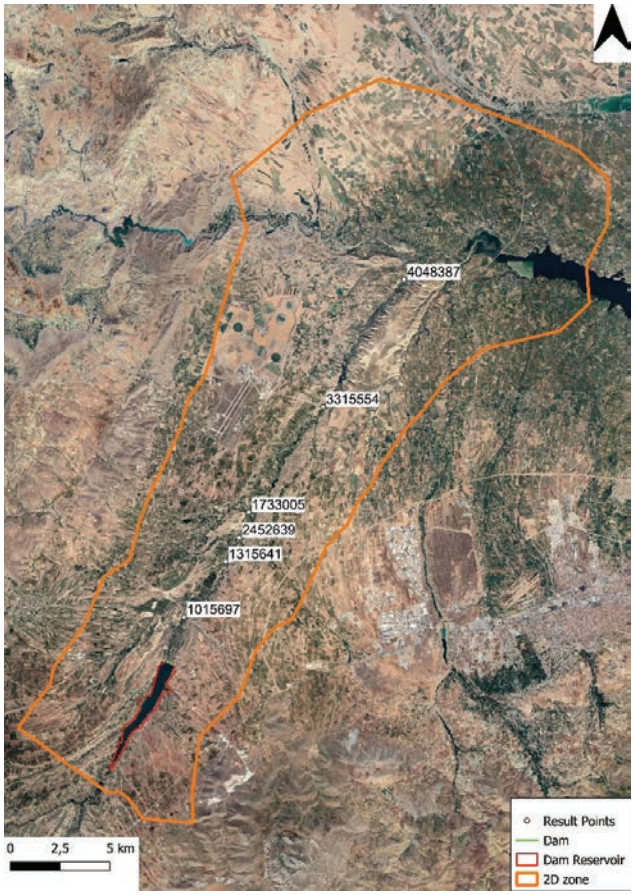

Figure 11. View of the geographical location of the result points.

downstream of the dam were determined and the velocity and depth profiles for these regions were examined in detail. The locations of these points in the study area are given in Figure 11.

The graphs of depth values in densely populated areas for all 5 scenarios are given in Figure 12.

In order to examine the behavior of the velocity limit in the region from the downstream of the Sultansuyu Dam to the Karakaya Dam reservoir, human density areas were determined. As the velocity limit increased, the depth values decreased. In fact, the result point 1015697 took the value of 0 when the maximum velocity limit increased to 15 m/s. In light of these results, it is seen that the increase in the velocity limit causes a decrease in the inundation area. The graphs of velocity values in densely populated areas for all 5 scenarios are given in Figure 13.

At the velocity limits of 3 m/s and 5 m/s at the successive and interconnected result points, the values are maximized at many points. However, as the limit increased to 15 m/s, the values became more significant. Up to the 10 m/s velocity limit, the result point 2452639 seems to have the highest values, while the result point 1315641 has higher values as the limit increases to 15 m/s. In light of these results, the velocity values in a streamflow decrease as the inundation area increases at lower velocity limits. Because the flow is limited to a velocity limit, the flow will tend to spread more and increase the inundation area. However, at more significant velocity limits and if the downstream of the dam behaves like a streamflow as in this study, higher velocity and lower inundation area will be observed. As illustrated in Figure 13, the temporal evolution of flow velocities indicates the flood arrival times at critical locations. For the downstream boundary at the Karakaya Reservoir confluence (Point 4048387), the flood wave arrives approximately 71 minutes after the breach in the 15 m/s scenario, demonstrating the rapid propagation of the flood front.

Comparison of Computation Times of Scenarıos

Models with complex topography or hydraulic structures may require the use of 2D or 3D hydrodynamic models [43]. GPUs, which provide high-performance computing (HPC) at low cost and low energy consumption, can also be used in hydrodynamic models, providing benefits in work areas involving many components [44]. In this study, for the model created in InfoWorks ICM, 5 scenarios were run using GPU under the same conditions. The simulations were performed on a workstation equipped with an AMD Ryzen 7 2700 Eight-Core Processor (3.2 GHz), 16 GB RAM, and an NVIDIA GeForce RTX 2070 GPU (8 GB VRAM). In this hardware environment, the scenario with a 3 m/s velocity limit was completed in 13120 seconds, for 5 m/s in 13317 seconds, for 10 m/s in 13411 seconds and for 15 m/s in 14339 seconds, and the un-capped (no velocity limit) reference simulation was completed in 15796 seconds. The results indicate a consistent trend where relaxing the velocity constraints increases computational effort. While the hydraulic results (maximum depth and inundation extent) of the un-capped scenario deviated by less than 1% from the 15 m/s scenario, the computation time increased by approximately 10% (1457 seconds) compared to the 15

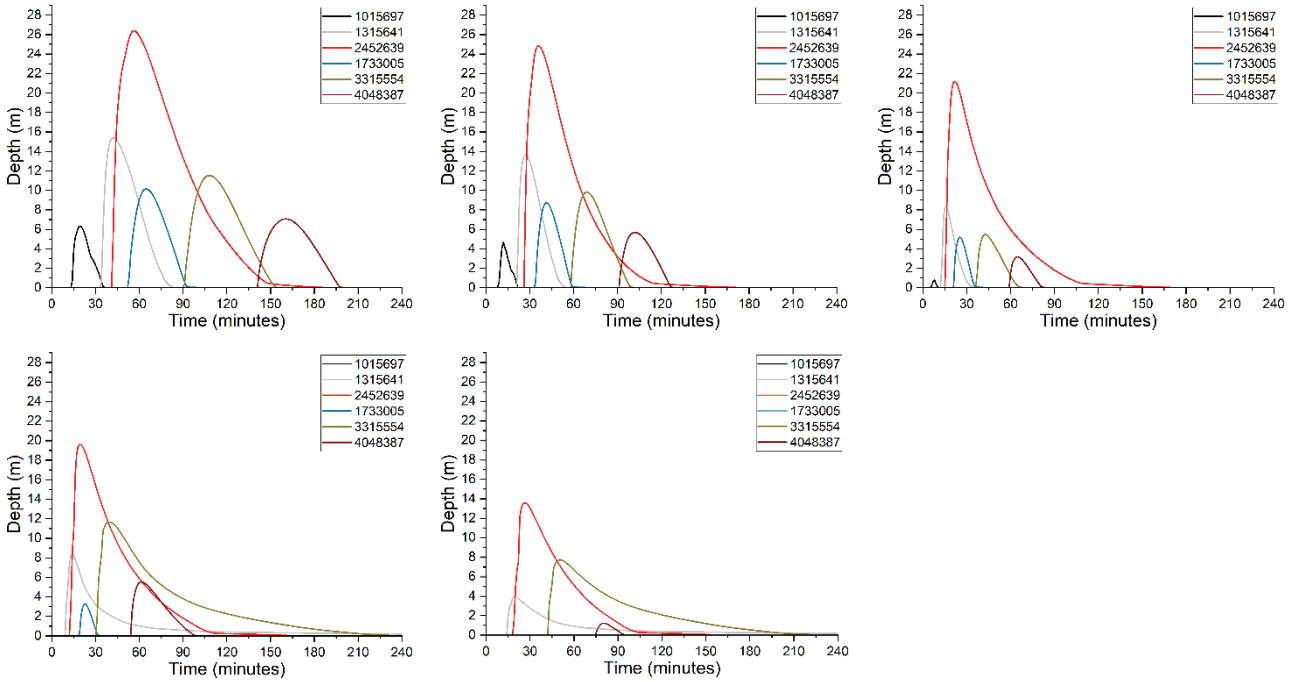

Figure 12. Change in depth values at selected result points with respect to time: a) 3 m/s, b) 5 m/s, c) 10 m/s and d) 15 m/s maximum velocity limit for 60 m dam levels, e) 15 m/s maximum velocity limit for 50 m dam levels.

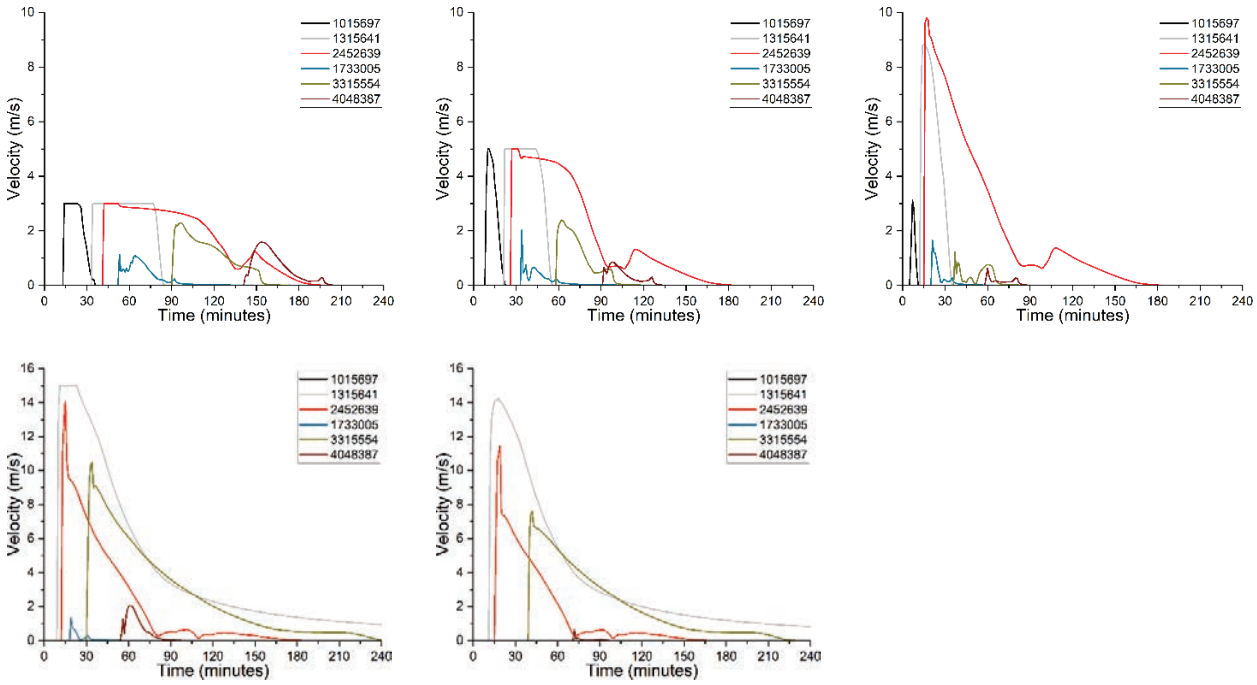

Figure 13. Change in velocity values at selected result points with respect to time: a) 3 m/s, b) 5 m/s, c) 10 m/s and d) 15 m/s maximum velocity limit for 60 m dam levels, e) 15 m/s maximum velocity limit for 50 m dam levels.

m/s case. This demonstrates that high velocity gradients in unconstrained flows force the solver to use smaller time steps to maintain stability, thereby increasing the computational load without providing meaningful improvements in accuracy. Therefore, velocity limit values are considered an important model parameter not only in physical terms but also in terms of numerical solution performance. Although the differences in computational time among the scenarios appear relatively small, these variations become critical in large-scale or long-duration simulations. In such cases, even minor increases in computational demand can significantly affect resource allocation, model optimization, and real-time decision-making in flood risk management. In addition, understanding how velocity constraints influence computational effort helps improve model efficiency, especially when applied to high-resolution domains or multi-breach analyses. In this context, it shows that there is a linear relationship between the maximum velocity limit and the computational times.

The hydrodynamic model employed in this study can be contextualized by comparing it with other widely used tools like HEC-RAS 2D and TELEMAC-2D. While HEC-RAS 2D is recognized for its robust capabilities in simulating flood wave propagation in semi-arid terrains [45], and TELEMAC-2D offers high flexibility for complex scenarios such as urban flood routing [46] and cascade reservoir scheduling [47], all high-resolution 2D hydrodynamic simulations inherently demand significant computational resources. In this context, the InfoWorks ICM platform utilized in this research distinguishes itself not by eliminating this cost, but by offering an integrated GPU-accelerated engine combined with flexible stability controls (such as the velocity limiters analyzed here). This combination allows for a more effective management of the trade-off between computational effort and numerical stability, particularly in emergency planning simulations where optimizing runtime is crucial.

CONCLUSION

In this study, the dam-break analysis of the Sultansuyu Dam, which was damaged by earthquakes of magnitude 7.8 (Mw) and 7.6 (Mw) in Kahramanmaraş province of Türkiye, was carried out. There are many agricultural lands downstream of Sultansuyu Dam in Malatya. The analysis was conducted using a hydrodynamic model developed with the InfoWorks Integrated Catchment Model software to simulate dam-break behavior and flood propagation. In the study, 5 different scenarios were created with 4 different velocity limits (3 m/s, 5 m/s, 10 m/s, and 15 m/s) at full dam water level and a velocity limit of 15 m/s based on the dam's water height of 50 m on the day of the earthquake. It was also investigated whether there is a correlation between velocity limit and calculation time in hydrodynamic models. As a result of the dam-break analysis, flood inundation maps, flood velocity maps, and flood hazard maps were created for 5 different scenarios. Finally, velocity and depth values were analyzed by taking result points from areas with high human density. The results based on the analysis of the simulations carried out in this research are as follows:

- The model was validated with a historical rainfall event. The statistical performance evaluation measures R^2=0.772, NSE=0.467, and RMSE= 0.136 m and the result are satisfactory.
- In the dam-break analysis, as the maximum velocity limits increased, the flow moved through a narrower cross-section. In other words, the spread of flood water decreased. The overtopping flood depth in the topography also decreased.
- According to the results of flood hazard maps, areas with hazard values greater than 2.5 for all scenarios are above 95% of all inundation areas. In other words, the hazard class in these areas is extreme and dangerous for everyone.
- Agricultural lands and discontinuous city structures downstream of the Sultansuyu Dam are also under threat in a possible dam break.
- Due to the fact that the flood water caused by the dam-break of Sultansuyu Dam reaches the region where the Tohma stream and the Karakaya Dam reservoir are located, the floodwaters spread all around at the junction point, flooding settlements and agricultural lands.
- The analysis revealed a direct correlation between the velocity limit threshold and computational effort. Relaxing the velocity limit from 3 m/s to 15 m/s resulted in a computational time increase of 1219 seconds. Furthermore, the un-capped (no limit) reference simulation required the longest runtime (15796 seconds), confirming that high-velocity flows demand smaller time steps for stability. Consequently, applying strictly defined velocity limits reduces the computational cost significantly while maintaining physical accuracy.

The study emphasizes that dam-break analysis should be performed in the planning and design of large water structures such as dams and possible measures should be taken accordingly. The study concluded that applying stricter (lower) velocity limits in hydrodynamic models significantly reduces the computational cost by preventing the excessive time-step reductions required for high-velocity stability. This study presents important practical implications for flood risk management and emergency response planning, particularly for structures exposed to earthquakes such as the Sultansuyu Dam. The resulting flood hazard maps can directly guide decision-makers in identifying floodwater distribution areas and high-risk areas. These results can form the basis for applications such as selecting locations for early warning systems, planning evacuation routes, and reorganizing agricultural activities. Furthermore, the information obtained through different velocity limit scenarios will provide a reference for risk analyses conducted on similar post-earthquake dams, guiding model optimization and computational efficiency. In this respect, the study not only provides a scientific contribution but also develops data-based recommendations applicable to engineering applications. From a practical perspective, the finding that 95% of the inundation zone falls under the extreme hazard category highlights the importance of reviewing downstream Emergency Action Plans to ensure they encompass such worst-case scenarios. The flood hazard maps generated in this study serve as valuable reference data for local authorities to evaluate evacuation corridors relative to high-velocity flood paths. Furthermore, for dams in seismically active zones, this study suggests that risk assessments could benefit from considering instantaneous failure scenarios to enhance preparedness for potential catastrophic events.

AUTHOR CONTRIBUTIONS

All authors contributed to the research conceptualization, methodology, and validation. Burak Çırağ conducted the formal analysis, developed the software, validated the results, performed the investigation, created visualizations, and wrote the original draft. Alp Ertuğrul Özer, Rıdvan Karagöz, Bilal Utancik and Alaaddin Özgüray Aydın contributed to the methodology, software development, data curation, and validation. Mahmut Fırat provided supervision, contributed to the conceptualization, methodology, and critically reviewed and edited the manuscript. All authors have read and approved the final manuscript.

DATA AVAILABILITY STATEMENT

The datasets generated and/or analyzed during the current study are available from various sources. The CORINE Land Cover data is publicly available from the Republic of Türkiye Ministry of Agriculture. Regarding the third-party data, the dam characteristics and high-resolution topographic data (DEM) were obtained from the General Directorate of State Hydraulic Works (DSI), and the meteorological dataset was obtained from the Türkiye Meteorology General Directorate (MGM); these datasets are not publicly available due to institutional regulations but can be accessed by researchers upon official application. Additionally, the InfoWorks ICM model input files, processed hazard maps, and simulation results generated during this study are available from the corresponding author on reasonable request.

CONFLICT OF INTEREST

The authors declare that they have no known competing financial interests or personal relationships that could have appeared to influence the work reported in this paper.

STATEMENT ON THE USE OF ARTIFICIAL INTELLIGENCE

Artificial intelligence was not used in the preparation of the article.

REFERENCES

[1] Azeez O, Elfeki A, Kamis AS, Chaabani A. Dam break analysis and flood disaster simulation in arid urban environment: The Um Al-Khair dam case study, Jeddah, Saudi Arabia. Nat Hazards 2020;100:995–1011. [CrossRef]

[2] Bharath A, Shivapur AV, Hiremath CG, Maddamsetty R. Dam break analysis using HEC-RAS and HEC-GeoRAS: A case study of Hidkal dam, Karnataka state, India. Environ Challenges 2021;5:100401. [CrossRef]

[3] Issakhov A, Borsikbayeva A. The impact of a multi-level protection column on the propagation of a water wave and pressure distribution during a dam break: Numerical simulation. J Hydrol 2021;598:126212. [CrossRef]

[4] Sesli H, Akköse M. Evaluation of sliding stability in concrete gravity dams using multiple wedge analysis. Sigma J Eng Nat Sci 2016;34:15–29.

[5] Molinari D, Menoni S, Ballio F, editors. Flood damage survey and assessment: New insights from research and practice. Hoboken, NJ: Wiley; 2017. [CrossRef]

[6] Munoz DH, Constantinescu G. 3-D dam break flow simulations in simplified and complex domains. Adv Water Resour 2020;137:103510. [CrossRef]

[7] Mao J, Wang S, Ni J, Xi C, Wang J. Management system for dam-break hazard mapping in a complex basin environment. ISPRS Int J Geo Inf 2017;6:162. [CrossRef]

[8] Tedla MG, Cho Y, Jun K. Flood mapping from dam break due to peak inflow: A coupled rainfall-runoff and hydraulic models approach. Hydrology 2021;8:89. [CrossRef]

[9] Al-Salahat M, Al-Weshah R, Al-Omari S. Dam break risk analysis and flood inundation mapping: A case study of Wadi Al-Arab Dam. Sustain Water Resour Manag 2024;10:74. [CrossRef]

[10] Abdulrahman KZ, Faris MR, Ibrahim HM, Yousif OS, Ghafoor AA, Othman LS, et al. Hypothetical failure of the Khassa Chai dam and flood risk analysis for Kirkuk, Iraq. Nat Hazards 2022;113:1833–1851. [CrossRef]

[11] Musa S, Adnan MS, Ahmad NA, Ayob S. Flood water level mapping and prediction due to dam failures. IOP Conf Ser Mater Sci Eng 2016;136:012084. [CrossRef]

[12] Sanz-Ramos M, López-Gómez D, Bladé E, Dehghan-Souraki D. A CUDA Fortran GPU-parallelised hydrodynamic tool for high-resolution and long-term eco-hydraulic modelling. Environ Model Softw 2023;161:105628. [CrossRef]

[13] Hou J, Kang Y, Hu C, Tong Y, Pan B, Xia J. A GPU-based numerical model coupling hydrodynamical and morphological processes. Int J Sediment Res 2020;35:386–394. [CrossRef]

[14] Tayfur G, Issakhov A, Zhandaulet Y. Numerical simulation of flow and dam body sediment over a movable bed due to an earthfill dam break. Sigma J Eng Nat Sci 2022;40:553–567. [CrossRef]

[15] DSI. Available from: https://www.dsi.gov.tr/. Accessed March 28, 2024.

[16] Cetin K, Cuceoglu F, Ayhan BU, Yildirim S, Aydin S, Demirdogen S, et al. Performance of hydraulic structures during 6 February 2023 Kahramanmaraş, Türkiye, earthquake sequence. Earthq Spectra 2024;87552930241258295. [CrossRef]

[17] Bayraktar A, Ventura CE, Yang TY, Hökelekli E, Taş Y. Observed damage behavior of earth dams during the 2023 Kahramanmaraş, Türkiye, earthquakes. Geotech Geol Eng 2024;1–16. [CrossRef]

[18] Hariri-Ardebili MA, Tosun H. Dams in the wake-up call of the 2023 Türkiye earthquake sequence: Insights from observed damages, risk assessment, and monitoring. Int J Disaster Risk Reduct 2024;102:104284. [CrossRef]

[19] SSB. Kahramanmaraş ve Hatay depremleri raporu. 2023. Available from: https://www.sbb.gov.tr/2023-kahramanmaras-ve-hatay-depremleri-raporu/. Accessed October 27, 2024.

[20] Tarım TV. Available at: https://www.tarimtv.gov.tr. Accessed on Oct 27, 2024.

[21] Ensonhaber. Available at: https://www.ensonhaber.com. Accessed on Oct 27, 2024.

[22] NTV. Available at: https://www.ntv.com.tr. Accessed on Oct 27, 2024.

[23] Cheng T, Xu Z, Hong S, Song S. Flood risk zoning by using 2D hydrodynamic modeling: A case study in Jinan City. Math Probl Eng 2017;2017. [CrossRef]

[24] Çırağ B, Fırat M. Taşkın yayılım haritalarında arazi kullanım türü ve yüzeysel akış etkilerinin değerlendirilmesi: Malatya ili örneği. Kahramanmaraş Sütçü İmam Univ Muhendis Bilim Derg 2022;25:222–236. [CrossRef]

[25] Alcrudo F, Mulet-Marti J. Urban inundation models based upon the shallow water equations: Numerical and practical issues. In: Finite Volumes for Complex Applications IV. 2005. p. 1–12.

[26] Çırağ B, Firat M. Two-dimensional (2D) flood analysis and calibration of stormwater drainage systems using geographic information systems. Water Sci Technol 2023;87:2577–2596. [CrossRef]

[27] Autodesk. Basic 2D hydraulic theory. 2024. Available at: https://help.autodesk.com/. Accessed on Apr 1, 2024.

[28] Wallingford H. R&D outputs: Flood risks to people, phase 2. Defra/Environment Agency Flood and Coastal Defence R&D Programme. PB No. 11545. 2006.

[29] Çırağ B, Karagöz R, Özer AE, Aydın AÖ, Fırat M. Modelling the dynamic performance of stormwater drainage systems integrated with infiltration trenches. Urban Water J 2025;22:244–257. [CrossRef]

[30] Dai Q, Zhu X, Zhuo L, Han D, Liu Z, Zhang S. A hazard-human coupled model (HazardCM) to assess city dynamic exposure to rainfall-triggered natural hazards. Environ Model Softw 2020;127:104684. [CrossRef]

[31] Nash JE, Sutcliffe JV. River flow forecasting through conceptual models part I-A discussion of principles. J Hydrol 1970;10:282–290. [CrossRef]

[32] Abdelkader M, Temimi M, Ouarda TB. Assessing the national water model's streamflow estimates using a multi-decade retrospective dataset across the contiguous United States. Water 2023;15:2319. [CrossRef]

[33] Avcı BC, Kesgin E, Atam M, Tan RI, Abdelkader M. Short-term climate change influence on surface water quality impacts from agricultural activities. Environ Sci Pollut Res Int 2023;30:89581–89596. [CrossRef]

[34] Ulu A. Application of response surface methodology in the optimisation of polymer concrete mechanical properties. Sigma J Eng Nat Sci 2024;42:1973–1985. [CrossRef]

[35] Rao KD, Shravya A, Dadhwal VK. A novel method of satellite based river discharge estimation using river hydraulic geometry through genetic algorithm technique. J Hydrol 2020;589:125361. [CrossRef]

[36] Çırağ B, Acar R, Katipoğlu OM, Yağanoğlu M, Şengül S. Reconstructing missing streamflow data in mountainous, snow-dominated regions using optimized hybrid machine learning. Water Resour Manage 2025;39:6165–6187. [CrossRef]

[37] Knoben WJ, Freer JE, Woods RA. Inherent benchmark or not? Comparing Nash-Sutcliffe and Kling-Gupta efficiency scores. Hydrol Earth Syst Sci 2019;23:4323–4331. [CrossRef]

[38] Çırağ B, Firat M, Aydin Ö. Analysis of the flood performance of stormwater drainage systems for different return periods. In: Proceedings of the International Conference on Contemporary Affairs in Architecture and Urbanism-ICCAUA. 2021;4:774–785. [CrossRef]

[39] Wang Y, Fu Z, Cheng Z, Xiang Y, Chen J, Zhang P, et al. Uncertainty analysis of dam-break flood risk consequences under the influence of non-structural measures. Int J Disaster Risk Reduct 2024;102:104265. [CrossRef]

[40] Khosravi K, Rostaminejad M, Cooper JR, Mao L, Melesse AM. Dam break analysis and flood inundation mapping: The case study of Sefid-Roud Dam, Iran. In: Extreme hydrology and climate variability. Amsterdam: Elsevier; 2019. p. 395–405. [CrossRef]

[41] Hayran S, Dönmez R, Karabacak T, Külekçi M. The reduction of greenhouse gas emissions and energy optimization in apricot production in Türkiye. Erwerbs-Obstbau 2023;65:1207–1216. [CrossRef]

[42] Mhmood HH, Yilmaz M, Sulaiman SO. Simulation of the flood wave caused by hypothetical failure of the Haditha Dam. J Appl Water Eng Res 2023;11:66–76. [CrossRef]

[43] Juez C, Lacasta A, Murillo J, Garcia-Navarro P. An efficient GPU implementation for a faster simulation of unsteady bed-load transport. J Hydraul Res 2016;54:275–288. [CrossRef]

[44] Ma Q, Liang S, Sun Z, Zhang R, Wang P. Development and evaluation of a GPU-based coupled three-dimensional hydrodynamic and water quality model. Mar Pollut Bull 2023;187:114494. [CrossRef]

[45] Karim IR, Hassan ZF, Abdullah HH, Alwan IA. 2D-HEC-RAS modeling of flood wave propagation in a semi-arid area due to dam overtopping failure. Civ Eng J 2021;7:1501–1514. [CrossRef]

[46] Li G, Shao W, Liu J. Simulation research of dam break flood in urban area based on TELEMAC-2D model. In: 2022 International Conference on Information Technology, Communication Ecosystem and Management (ITCEM). IEEE; 2022. p. 86–89. [CrossRef]

[47] Liao T, Wei R, Zhou L, Min J. Simulation of reservoir scheduling in cascade dam-break analysis with TELEMAC-2D. In: 30th TELEMAC User Conference; 2024 Oct 8–10; Chambéry, France.